crystals

MDPI

Article

Stable Photocatalytic Paints Prepared from Hybrid Core-Shell Fluorinated/Acrylic/TiO_2 Waterborne Dispersions

Audrey Bonnefond [1], Edurne González [1], José M. Asua [1], Jose Ramon Leiza [1,*], Eliana Ieva [2], Giulio Brinati [2], Serena Carella [2], Alessio Marrani [2], Alessandro Veneroni [2], John Kiwi [3], Cesar Pulgarin [3] and Sami Rtimi [3]

1 Polymat, Kimika Aplikatua Saila, Kimika Zientzien Fakultatea, University of the Basque Country UPV/EHU, Joxe Mari Korta Zentroa, Tolosa Hiribidea 72, 20018 Donostia-San Sebastián, Spain; a-bonnefond@hotmail.fr (A.B.); edurne.gonzalezgandara@gmail.com (E.G.); jm.asua@ehu.eus (J.M.A.)

2 Solvay Specialty Polymers Italy, Viale Lombardia 20, 20021 Bollate, Italy; eliana.ieva@solvay.com (E.I.); giulio.brinati@solvay.com (G.B.); serena.carella@solvay.com (S.C.); alessio.marrani@solvay.com (A.M.); alessandro.veneroni@solvay.com (A.V.)

3 Ecole Polytechnique Federale de Lausanne, EPFL-SB-ISIC-GPAO, Station 6, CH-105, Switzerland; john.kiwi@epfl.ch (J.K.); cesar.pulgarin@epfl.ch (C.P.); sami.rtimi@epfl.ch (S.R.)

* Correspondence: jrleiza@ehu.eus; Tel.: +34-943-015-329; Fax: +34-943-017-065

Academic Editors: Roberto Comparelli, Lucia Curri and Marinella Striccoli
Received: 25 July 2016; Accepted: 19 October 2016; Published: 24 October 2016

Abstract: The contamination of air and water is one of the major concerns towards the development of a sustainable world in the 21st century. In this context many efforts are devoted to the design of photocatalytic paints able to degrade chemical and biological impurities present in air and water. In this work, the photocatalytic activity of hybrid films formed from the blends of pure acrylic or core/shell fluorinated/acrylic waterborne dispersions and photocatalytic titanium dioxide (TiO_2) nanoparticle dispersions was first assessed. The films show photocatalytic activity (inactivation of the *Escherichia coli* bacteria under UV irradiation) at the substrate-film interface, but very reduced activity in the air-film interface due to the substantially lower amount of the TiO_2 nanoparticles in the vicinity of this interface. In a second step, the fluorinated/(meth)acrylic core-shell hybrid dispersions were used as binders in the formulation of waterborne photocatalytic paints and the stability of the paints, in terms of gloss retain and color change, was assessed during 5000 hours of accelerated weathering tests (QUV-B). Although a decrease in gloss retention and increased color change occurs during the first 1000 hours of exposure, no further change of these properties takes place, which is an excellent indication of stable photocatalytic paints.

Keywords: photocatalytic paints; titanium dioxide nanoparticles (TiO_2); accelerated weathering; film morphology; gloss and color

1. Introduction

The recent awareness of the threat to human health and to the environment of air and water pollutants has led scientists to search for a new technology able to reduce the contaminants' concentrations. In the last two decades, and after the discovery of the properties of photocatalytic metal oxide nanoparticles (NPs) in the degradation of pollutants, the interest in the development of photocatalytic self-cleaning paints and coatings has increased enormously in academia and industry [1–3]. The mechanism of self-cleaning paints is based on the presence of a photocatalyst (commonly composed of metal oxide NPs) that, under UV light exposure, exceeds its band gap energy and generates electron hole pairs. Although, in most cases, the electron hole pairs recombine to

generate heat, in some cases the photocatalytic phenomena takes place and electrons and holes reach the surface of the photocatalyst where they can participate in redox reactions with the present oxygen and water molecules, creating highly active radicals. These radicals are able to decompose organic compounds and bacteria and, thus, they are able to clean surfaces [4–6]. Furthermore, since the surface of the photocatalyst becomes superhydrophilic under UV irradiation, it is also claimed that photocatalytic materials might also have self-cleaning properties [7].

Among the different photocatalysts, titanium dioxide (TiO_2) is the most thoroughly used because of its low toxicity, chemical stability, low cost, abundance as a raw material, and its high photocatalytic efficiency [8]. Nonetheless, self-cleaning paints with other metal oxides, like ZnO, have also been reported [9,10].

A conventional waterborne paint is prepared in two steps. In the first step, the dispersion of the pigment in water, stabilizer, thickener, and auxiliary solvents, so-called mill base, is prepared. The pigment can be composed by non-photocatalytic TiO_2 (rutile rich) and other inorganic materials, like calcium carbonate, depending on the final application and price sought for the paint (e.g., indoor or outdoor use). In the second step, the mill base is blended with the binder (polymer latex) and the paint is obtained. Waterborne photocatalytic paints differ from conventional waterborne paints in the addition of the photocatalyst (anatase phase rich TiO_2 NPs) in the formulation. There is little information in the scientific literature about the preparation of photocatalytic paints, the way the photocatalyst is incorporated, and its final distribution on the paint film.

Commercial photocatalytic paints are mostly implemented in exterior (as façade paints) to avoid soiling and to keep the surface of the buildings clean [11]. More recently, indoor photocatalytic paints have also been implemented with the aim to control the odour, degrade volatile organic compounds (VOC) and NO_X compounds, and maintain surfaces free of bacteria and fungi [9,12–16], among other applications.

Hochmannova and Vytrasova [9] found that the photocatalytic activity of coatings was influenced by the type of acrylic dispersion used as a binder, the total pigment volume concentration (PVC), the type of the photocatalytic nanoparticles, and by the morphology of the surfaces.

Nevertheless, one of the most controversial aspects of the photocatalytic paints is related with the potential degradation of the organic binder constituents during long exposure to UV irradiation. Thus, there are works that show that under UV light irradiation the organic binder in the photocatalytic paint degrades forming other stable compounds, like acetaldehydes and ketones, which do not proceed to further mineralization [17], or carbonyls [18]. Other authors [19] also reported leaching of the TiO_2 NPs from the paint matrix to the environment during very long periods of UV exposure (one year) although the measured values were considered low (1.5 $\mu g/dm^3$ in a climate chamber, and between 0.5 and 14 $\mu g/dm^3$ during leaching tests). The detachment of the NPs was observed in photocatalytic paints that contained TiO_2 NPs, but this was not observed in paints that only contained the usual TiO_2 pigment. This behaviour was attributed to a weaker binding of the TiO_2 NPs to the polymer matrix, which was observed in the scanning electron microscope (SEM) images of the surface of the paints.

In this context, Baudys et al. [10] interestingly pointed out that the key point in the development of stable paints is the creation of better barriers to the photocatalytic mineralization process, so that the polymer binder remains intact longer and the paint exhibits an appreciable lifetime as a coated film. They noted that in the preparation of photocatalytic paints it is important to find a compromise between maintaining a reasonable degree of photocatalytic activity whilst retaining a good paint stability. Clearly, the higher the photocatalytic activity of the paint, the lower the paint lifetime due to the light-induced weathering and photo-chalking.

In this work, photocatalytic paints were formulated using two types of polymeric binders (a pure (meth)acrylic latex (LM1) and a fluorinated/(meth)acrylic latex (CS2) with core-shell morphology) and two types of photocatalytic TiO_2 NPs (Degussa P25 and a sample from Johnson and Matthey (JM)). First, hybrid dispersions were prepared by blending the photocatalytic TiO_2 aqueous dispersions and the latexes. Polymer films were prepared and their photocatalytic activity was assessed by analyzing

the inactivation of *Escherichia coli* bacteria. The photoactivity was found superior in the substrate-film interface due to the higher concentration of the TiO_2 in the bottom of the film. Then, the stability of the photocatalytic paints formulated with a hybrid binder composed by the fluorinated/(meth)acrylic core-shell latex and JM TiO_2 was analyzed by measuring the evolution of gloss retention and color change during the exposure of coated aluminum panels to accelerated weathering tests (QUV-B) for 5000 hours. Both gloss and color decreased during the first 1000 hours of exposure and then remained constant at acceptable values.

2. Results and Discussion

2.1. Characterization of the Films Obtained by Casting the Blends

Figure 1 presents two SEM images of the cross-sections of the films made with blends of latex LM1 cast on glass. The SEM images show large aggregates of TiO_2 NPs dispersed in the acrylic polymer matrix. The top areas of the films were less concentrated in TiO_2 than the bottom. This was confirmed by X–ray photoelectron spectroscopy (XPS) analysis carried out at both interfaces of the films (see Table 1); no titanium was found at the air-film interface, while the analysis at the film-substrate interface revealed the presence of titanium.

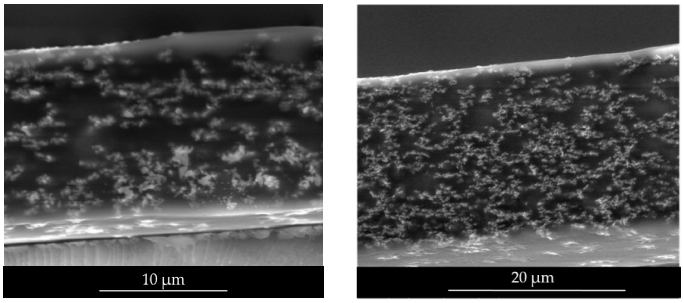

Figure 1. SEM micrographs of films cast on glass for the LM1 + P25 (**left**) and LM1 + JM (**right**) blends (both containing 10 weight percent by polymer (wbp%) TiO_2).

Table 1. XPS determination of % Ti of Atomic Ti both interfaces of the films obtained by casting the LM1 + P25, LM1 + JM, CS2 + P25, and CS2 + JM blends prepared with 10 wbp% TiO_2.

Sample	Interface	% Atomic Ti
LM1 + P25	Air-film interface	0
	Film-substrate interface	0.6
LM1 + JM	Air-film interface	0
	Film-substrate interface	1.9
CS2 + P25	Air-film interface	0
	Film-substrate interface	0.3
CS2 + JM	Air-film interface	0
	Film-substrate interface	0.5

Cross-sections of the films obtained by casting the blends into silicon molds were also analyzed by transmission electron microscopy (TEM) (Figure 2). The images show that the TiO_2 NPs formed large aggregates in the films, in agreement with the SEM images. No noticeable differences between the two types of TiO_2 NPs were observed. Note that in the enlargement of the cross-sectioned film for the blend CS2 + JM presented in the supporting information (Figure S4) it can clearly distinguish the core-shell structure of the latex particles. The dark domains correspond to the fluorinated polymer and the white domains to the acrylic film forming polymer.

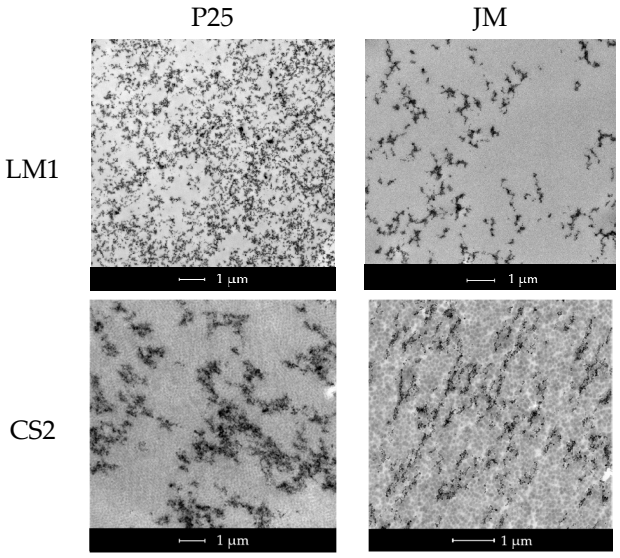

Figure 2. TEM micrographs of the cross-sections of films obtained by casting the LM1 + P25, LM1 + JM, CS2 + P25, and CS2 + JM blends prepared with 10 weight percent by polymer (wbp%) TiO_2.

These results demonstrate that the high density of TiO_2 NPs caused a non-homogeneous distribution of NPs throughout the films. TiO_2 NPs accumulate preferentially at the bottom of the film leaving the top surface almost free of TiO_2 NPs. This morphology might affect the catalytic activity of the films since little active material is available at the air-film surface.

2.2. Photocatalytic Activity of The Films Obtained by Casting the Hybrid Blends

The photocatalytic activity of the films prepared by casting the hybrid blends on silicone molds was assessed by the degradation of *Escherichia coli* under UV radiation. The *Escherichia coli* inactivation kinetics were measured at both interfaces of the films and the results are presented in Figure 3. For the sake of comparison, the results obtained for the films prepared without TiO_2 (blank samples LM1 and CS2) are also presented. The *Escherichia coli* inactivation measured at the air-film interface was very similar and low for all the samples. However, when the *Escherichia coli* was deposited in the substrate-film interface, films containing TiO_2 were able to completely degrade the *Escherichia coli* (seven orders of magnitude in the concentration). This result is in agreement with the non-homogeneous distribution of the TiO_2 NPs previously observed by SEM (Figure 1) and XPS (Table 1). The kinetics of the degradation of *Escherichia coli* in the substrate-film interface is comparable, but clearly slower than in films produced from TiO_2 nanoparticle Pickering-stabilized (meth)acrylic latexes [20,21].

2.3. Photocatalytic Waterborne Paints

Photocatalytic paints were formulated using the hybrid blends as the binder as discussed above. For the sake of brevity only photocatalytic paints produced with the core-shell latexes (CS2 + JM and CS2 + P25) are discussed here. For comparative purposes a neat latex (CS2) was also used to prepare paint without photocatalytic TiO_2 NPs. Note that in the formulation of the paints (the details of the formulation are given in the Materials and Methods section) non-photocatalytically active TiO_2 (rich in rutile phase) was also used as a pigment. The paints were cast in panels and the performance (stability of the paint) of the coated panels was assessed by exposing them to accelerated weathering tests (QUV-B) for 5000 hours and analyzing gloss retention and color change. Degradation of pollutants was not assessed for the paints as it was already proved that the films made from the blends presented photocatalytic activity.

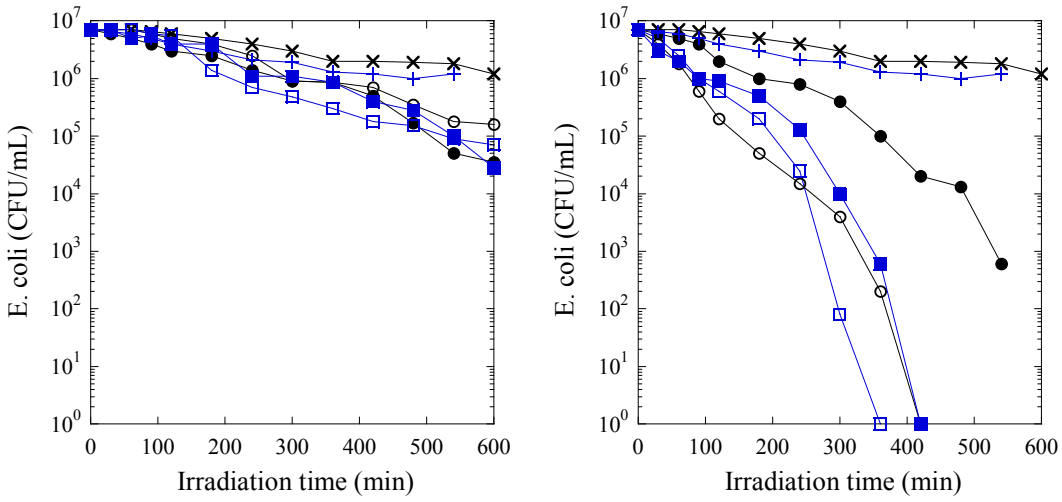

Figure 3. *Escherichia coli* inactivation kinetics for × LM1, ○ LM1 + P25, ● LM1 + JM, + CS2, □ CS2 + P25 and ■ CS2 + JM prepared with 10 wbp% TiO_2 at (a) air-film interface and (b) film-substrate interface.

Figure 4 displays the pictures of the aluminum panels coated with formulated paints containing the latex CS2 and the latex CS2 mixed with 10 wbp% (weight percent by polymer) TiO_2 NPs from JM as binders. Both paints were formulated with high weather-resistant rutile TiO_2 pigment. The quality of the paints was good regardless of the presence of the photocatalytic TiO_2 NPs from JM.

Figure 4. Pictures of the aluminum panels coated with formulated paints containing (**a**) CS2 and (**b**) CS2 + JM (10 wbp%) as binders.

Figure 5 shows the evolution of gloss retention and color change during the 5000 hours of QUV-B exposure (the results of the core-shell latex CS2 + P25 are displayed in Figure S1). Most of the samples presented the same behavior. A significant drop in gloss retention was observed after 1000 hours and then it remained constant until the end of the test (samples with 1 and 5 wbp% TiO_2). A similar behavior is usually observed in architectural coatings and it is associated with the degradation of the acrylic phase and additives. Interestingly, the panel with 10 wbp% TiO_2 behaved somewhat differently. The gloss decayed faster during the first 500 hours but then it remained constant at substantially higher gloss values than the rest of the cases (similar to the control panel). It seems that the faster degradation of the acrylic binder and other additives is likely due to the higher concentration of TiO_2. This may be due the TiO_2 NPs being exposed faster to the paint surface, then stopping further degradation, as in

the other cases. Regarding the color change (see Figure 5b), all of the samples showed a large jump after 500 hours of exposure and then no significant changes were evidenced. The step change at the beginning of the weathering test could be associated with degradation of the additives added to the formulation. The panel with the higher photocatalytic TiO_2 content showed a lower color change.

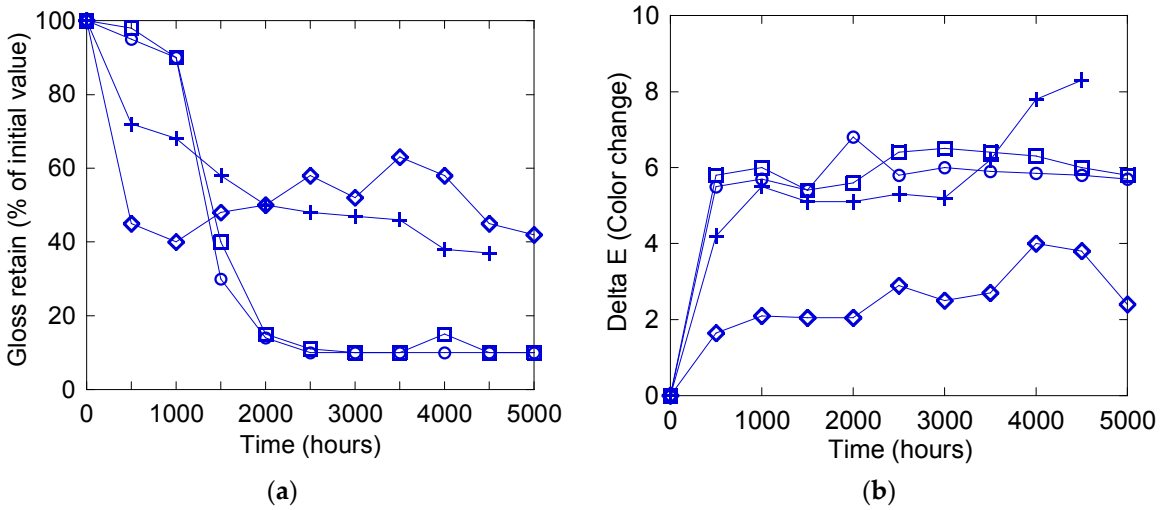

Figure 5. Time evolution of (**a**) gloss retention and (**b**) color change after exposure of UV-B of the different coated panels for samples + CS2, ○ CS2 + JM (1 wbp%), □ CS2 + JM (5 wbp%), and ◊ CS2 + JM (10 wbp%).

At the end of the weathering tests, samples were analyzed by SEM to study the evolution of the surface morphology during the QUV-B exposure (see Figure 6 for the core-shell latex CS2 + JM and Figure S2 for the core-shell latex CS2 + P25).

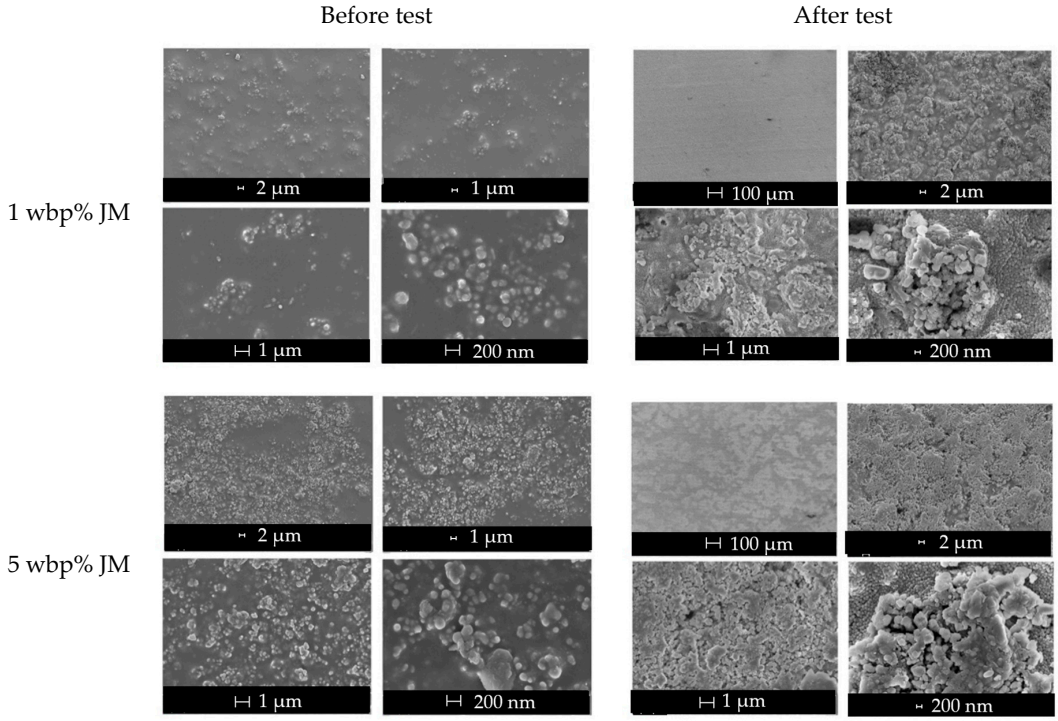

Figure 6. SEM micrographs of the surface of the panels coated with formulated paints containing CS2 + JM as binders before and after the weathering tests, at different magnifications.

Figure 6 shows that a significant aggregation of particles was observed at the surface of all of the panels before the weathering test. Taking into consideration that panels coated with paints formulated without the TiO_2 pigment presented very smooth surfaces (as shown in the supporting information in Figure S3), it can be concluded that this aggregation was only due to the pigment added to formulate the paint. Nonetheless, particle aggregation increased with the amount of photocatalytic TiO_2 NPs in the binder. Photocatalytic TiO_2 NPs may increase the ionic strength of the system, decreasing the stability of the paint and, consequently, increasing particles' aggregation.

After the weathering test, the increase in the surface roughness was evident. This is coherent with the drop in gloss observed in Figure 5a and can be explained by the acrylic phase and additives degradation (note that it has already been reported in the literature that Polyvinylidene fluoride (P(VDF)) is not likely to be degraded [22]). However, it should be remarked that, after this initial drop, the curves remain constant, which can be taken as an indication that further degradation of the polymer was substantially minimized.

As a conclusion, although the photocatalytically active TiO_2 NPs (present in the hybrid blends) were not present at the air-film interface of the paint at the beginning of the test, the degradation of the acrylic phase after some QUV-B exposure allowed the TiO_2 NPs which were located close to the surface of the paint to reach the air-film interface. The presence of the photocatalytically active TiO_2 NPs at the surface of the paint, together with its higher roughness, are the keys to get a paint with good photocatalytic activity toward pollutant degradation [20,21].

3. Materials and Methods

3.1. Materials

Methyl methacrylate (MMA, Quimidroga, Spain), *n*-butyl acrylate (BA, Quimidroga, Spain), and methacrylic acid (MAA, Aldrich, Spain) monomers were used as received. The P25 and JM TiO_2 NPs were kindly provided by Degussa and Johnson and Matthey, respectively. Potassium persulfate (KPS, Sigma, Spain), tert-butyl hydroperoxide (TBHP, Sigma-Aldrich, Spain), and ascorbic acid (AsAc, Sigma-Aldrich, Spain) were used as initiators. Sodium lauryl sulfate emulsifier (SLS, Sigma, Spain) was used as received. Ammonium hydroxide (NH_4OH, Sigma, Spain) was employed as a base. Doubly-deionized (DDI, MilliQ quality) water was used throughout the work.

The P(VDF-*co*-HFP) (88.2/11.8 wt%) seed latex employed for the synthesis of the core-shell NPs was provided by Solvay Specialty Polymers (Italy). The solids content of the latex was 31 wt% and the average diameter of particles was 102 nm.

3.2. Synthesis of the Acrylic Latex LM1

The acrylic latex was synthesized by a seeded semi-batch emulsion polymerization reaction carried out in a 1 L jacketed reactor equipped with a reflux condenser, nitrogen inlet, a sampling device, and a stainless steel anchor stirrer rotating at 250 rpm. The formulation used to prepare the seed is given in Table 2. The organic phase containing the monomers was added to the aqueous phase composed of the emulsifier dissolved in water and the resulting dispersion was charged into the reactor. The temperature was increased to 70 °C and once the temperature was reached, the initiator (potassium persulfate, KPS) was added in a shot. The final solids content of the seed was 20 wt% and the average diameter of particles was 74 nm. The seeded semi-batch emulsion polymerization was prepared following the recipe given in Table 3. The seed was diluted with water to reach a solids content of 1.3 wt% and then a pre-emulsion containing the mixture of monomers, water, and emulsifier, an aqueous phase containing the oxidant (tert-butyl hydroperoxide, TBHP), and another one containing the reductant (ascorbic acid, AsAc), were fed using three different streams to the reactor for 4 h. After the feed period had finished, the system was left to react for one more hour and the temperature was decreased. The final solids content of the LM1 latex was 50 wt% and the final diameter of particles was 332 nm.

Table 2. Formulation used for the preparation of the seed.

Compound	Charge (wt%)
MMA/BA (50/50 wt %)	20
Water	80
SLS *	0.8
KPS *	1

* With respect to the monomer.

Table 3. Formulation used for the preparation of the latex LM1.

Compound	Charge (wt%)
Seed + water	40
MMA/BA/MAA (49.5/49.5/1 wt %)	53
Water	7
SLS *	0.48
TBHP/AsAc (2/1 mol/mol) *	1

* With respect to the monomer feed.

3.3. Synthesis of The Core-Shell Latex Cs2

The core-shell latex CS2 was synthesized by seeded semi-batch emulsion polymerization following the recipe presented in Table 4. First, the P(VDF-*co*-HFP) seed latex provided by Solvay Specialty Polymers (Italy) was loaded in a 1 L jacketed reactor equipped with a reflux condenser, nitrogen inlet, a sampling device, and a stainless steel anchor stirrer rotating at 250 rpm, and the temperature was increased to 70 °C. Once the temperature was reached, a pre-emulsion containing the mixture of acrylic monomers, water, and emulsifier, an aqueous phase containing the oxidant (TBHP), and another one containing the reductant (AsAc), were fed using three different streams to the reactor for 3 h. After the feed period had finished, the system was left to react for one more hour and the temperature was decreased. The final solids content of the core-shell latex was 40 wt% and the final average diameter of particles was 140 nm.

Table 4. Formulation used for the synthesis of the core-shell latex CS2.

Compound	Charge (wt%)
PVDF/HFP seed	59
MMA/BA/MAA (49.5/49.5/1 wt%)	22
Water	19
SLS *	1
TBHP/AsAc (2/1 mol/mol) *	1

* With respect to the monomer feed.

3.4. Preparation of The Hybrid Blends

Two different latexes were used in order to prepare the hybrid blends. On the one hand, a conventional (meth)acrylic latex (poly(methyl methacrylate-*co*-butyl acrylate-*co*-methacrylic acid), P(MMA-*co*-BA-*co*-MMA), 49.5 wt% MMA, 49.5 wt% BA, and 1% wt MAA) commonly used for coating applications was employed (labeled as LM1). As acrylic polymers may suffer degradation under UV exposure [17,18,23], a core-shell latex containing perfluorinated polymer in the core was also used in order to improve the UV resistance of the final blends. P(VDF) is a high molecular weight polymer used in architectural applications due to its exceptional weathering resistance: indeed, the presence of strong C-F bonds allows the polymer to resist against the photo-oxidation initiated by UV light [24,25]. The core-shell latex was produced by seeded semi-batch polymerization using as seed a poly(vinylidene fluoride-*co*-hexafluoro propene) (P(VDF-*co*-HFP) latex (provided by Solvay Specialty

Polymers, Italy) and copolymerizing a mixture of MMA/BA/MAA (49.5/49.5/1 wt%) on the shell to produce a film forming latex (labeled as CS2). It is worth pointing out that the P(VDF-*co*-HFP) latex is not film-forming by itself due to its high Tg (well above room temperature) and partial crystallinity. Thus, a shell of a film-forming acrylic polymer is produced to render the composite latex the ability to form a film at room temperature (see Figure S4, supporting information). Note that both latexes (LM1 and CS2) contain 1 wt% of MAA in the formulation to obtain carboxylic acid surface functionalized polymer particles. The pH of both latexes was adjusted to 10 by the addition of NH_4OH, in order to deprotonate the carboxylic acid groups at the surface of the particles and to obtain negatively charged polymer particles ($pKa^{COOH} \approx 4.15$). The deprotonated carboxylic acid groups play a key role in the interaction with the TiO_2 surface to obtain stable blends.

For the preparation of the blends, different amounts of TiO_2 NP aqueous dispersions at pH = 2 were added to the latexes at pH = 10, and left overnight under stirring. The final pH of the blends was close to 9. At this pH, both the polymer particles and the TiO_2 NPs were negatively charged and the final blends obtained were stable and form good films (see Figure 7). The amounts of TiO_2 in the final blends were 1, 5, and 10 wbp%.

Figure 7. Film obtained by casting the blend LM1 + P25 (containing 10 wbp% TiO_2).

3.5. Characterization of the TiO_2 NPs

In this work, two different aqueous dispersions of TiO_2 NPs containing 2.5 wt% TiO_2 were employed for the preparation of the blends. TiO_2 NPs were named P25 (Degussa P25 TiO_2) and JM (Johnson and Matthey TiO_2). Although the theoretical particle diameters were 20 and 30 nm for P25 and JM, respectively, the diameter measured experimentally by dynamic light scattering (DLS) in the aqueous dispersions after 20 min of sonication using a Branson 450 w (operating at 8-output control and 60% duty cycle) were 150 and 70 nm, respectively. These results indicate that there was some aggregation of the TiO_2 NPs in the aqueous dispersions. The isoelectric point (IEP) of the TiO_2 NPs (measured by zeta potential measurements using DLS) were 7 and 6 for P25 and JM, respectively. The pH of the TiO_2 NPs dispersions was around 2 in both cases, so the TiO_2 NPs were positively charged.

3.6. Latex and Film Characterization.

Dynamic light scattering (Zetasizer Nano ZS, Malvern Instruments, Worcestershire, UK) was used to measure the z-average diameter of the TiO_2 NP dispersion, mini-emulsion droplets, and final polymer particles.

The morphology of the films obtained by casting the latexes onto silicon molds was analyzed by transmission electron microscopy (TEM) (FEI, Eindhoven, The Netherlands) in a TECNAI G2 20 TWIN (FEI) operating at an accelerating voltage of 200 kV in a bright field image mode. The films cast at room temperature were trimmed at −40 °C using an ultramicrotome device (Leica EMFC6, Viena,

Austria) equipped with a diamond knife. The ultrathin sections (100 nm) were placed on 300 mesh copper grids and were observed without further staining.

SEM (FEI, Eindhoven, Netherlands) analysis was performed in a Quanta 250 (FEI) in the low vacuum mode at 10 kV and using a long field detector. Samples were dipped into liquid N_2 to get fractures and they were adhered to stubs for cross-section analysis.

X-ray photoelectron spectroscopy (XPS) composition data and spectra were acquired on a SPECS (SPECS, Berlin, Germany) instrument equipped with a Phoibos 150 1D-DLD analyzer (SPECS, Berlin, Germany) and a monochromatic Al Kα X-ray source (SPECS, Berlin, Germany). Compositional survey and detail scans were acquired using a pass energy of 80 eV. High resolution spectra were acquired using a pass energy of 30 eV. The above data were taken at 90° takeoff angle. Data analysis was performed with Casa XPS 2.3.16 software (Casa Software Ltd, Cheshire, UK) to fit the signals to Gauss-Lorentzian curves, after removing the background (Shirley).

3.7. Formulation of the Photocatalytic Paints

For the formulation of the paints, first the pigment grind was prepared in a high speed mixer with glass beads following the recipe given in Table 5, and then it was mixed with the other ingredients employed for the formulation of the paints (see Table 6). Once the formulated paints were obtained, they were applied on aluminum panels with a drawdown bar and let to dry at room temperature.

Table 5. Formulation of the pigmented grind employed in the formulation of the paints.

Compound	Weight (g)
Pigment TiO_2 Dupont R-960	15
Biocite	1.1
Dispersant	0.5
Defoamer	0.2
Water	59

Table 6. Formulation employed for the accelerated weathering test.

Compound	Weight (g)
Binder (latex CS2 + TiO_2)	50
Coalescent	2.5
Dispersant	0.5
Pigment grind	15
% solid	46

3.8. Evaluation of the Bacterial Inactivation on Prepared Polymers under Solar Light Irradiation

Escherichia coli (*E. coli* K12) was obtained from Deutsche Sammlung von Mikroorganismen und Zellkulturen GmbH (DSMZ) ATCC23716 (Braunschweig, Germany). The 200 µL culture aliquots with an initial concentration of ~10^6 CFU·mL^{-1} in NaCl/KCl (pH 7) were placed either at the air-film or at the film-substrate interface. The polymeric sample area was 9 cm^2. The polymer permits a homogeneous distribution of the inoculum evenly without needing an adsorption stage. A well-dispersed non-heterogeneous contact was established between the film and the bacterial solution. The 200 µL of the *Escherichia coli* solution was exposed at room temperature (25–28 °C). The films were then placed on Petri dishes provided with a lid to prevent evaporation. The used Petri dishes were selected according to their absorption edge. In our case they do not absorb the emitted light during our experiment.

After each pre-defined irradiation time, the films were transferred into sterile 10 mL tubes containing 5 mL autoclaved NaCl/KCl saline solution. This solution was subsequently mixed thoroughly using a vortex for 3 min. Serial dilutions were made in NaCl/KCl solution. A 100 µL

sample of each dilution was pipetted onto a nutrient agar plate and then spread over the surface of the plate using the standard plate method. Agar plates were incubated lid down, at 37 °C, for 24 h before colonies were counted. To verify that no bacteria remained adsorbed to the polymeric surface, films were incubated on agar Petri dishes overnight. Almost no bacterial re-growth was observed as adhered bacteria to the polymeric surface. Samples were irradiated in the cavity of a Suntest solar simulator light CPS (Atlas GmbH, Hanau, Germany) at a light dose of 55 mW/cm^2. The washing solution was a NaCl/KCl saline solution (8 g/L NaCl and 0.8 g/L KCl) followed with a MQ-water wash. Three independent assays were done for each sample. The statistical analysis of the results was performed for the colony-forming unit (CFU) values calculating the standard deviation values (n = 5%). The average values were compared by one-way analysis of variance and with the value of statistical significance. The one-way analysis of variance (one-way ANOVA) was used to compare the mean of the samples using the Fisher distribution.

3.9. Accelerated Weathering Test

QUV-B weathering tests were performed on the formulated paints coated on aluminum panels. Although the results produced by UV-A are closer to that of sunlight, the UV-B lamp is the most widely used fluorescent light source when durable materials are studied because the degradation takes place at faster rates [26]. The tests lasted 5000 hours in total and cycles were as follow: eight hours of UVB-313 at 70 °C and four hours of humidity in the absence of irradiation (ASTM D 4329-84). Among the different properties that could be checked to determine the coating durability, it was decided to focus on color and gloss. Every 500 hours panels were taken out of QUV and the coating properties were measured. Moreover, a visual inspection of the film was made in order to check if chalking or other types of degradation forms were present.

4. Conclusions

This paper describes the preparation of photocatalytic paints using two types of polymeric binders (a pure (meth)acrylic latex and a fluorinated/(meth)acrylic latex with core-shell morphology) and two types of photocatalytic TiO_2 nanoparticles. First, the photocatalytic activity of the TiO_2 nanoparticles embedded in a polymeric matrix was assessed by analyzing the inactivation of *Escherichia coli* bacteria on films produced from hybrid dispersions obtained by blending the TiO_2 aqueous dispersions and each of the latexes. The photoactivity was measured in both surfaces (air-film and substrate-film) and it was found superior in the substrate-film interface due to the higher concentration of the TiO_2 nanoparticle aggregates in the bottom of the film that was clearly visualized in cross-sections analyzed by SEM, and quantitatively measured by XPS.

The formulated photocatalytic paints were analyzed in terms of stability by measuring the evolution of gloss retention and color change during the exposure of the coated panels to accelerated weathering tests (QUV-B) for 5000 hours. Both gloss retention and color change decreased during the first 1000 hours of exposure and then remained constant at acceptable values. Interestingly, the panel with the highest concentration of photocatalytic TiO_2 (10 wbp%) showed a faster decay of these properties to reach higher constant values. This was attributed to the faster degradation of the organic compounds in the paint (acrylic binder and additives) and faster exposure of the TiO_2 NPs to the paint surface stopping further degradation of the paint.

Supplementary Materials: The following are available online at http://www.mdpi.com/2073-4352/6/10/136/s1, Figure S1: (a) Gloss retain and (b) color change after UV-B exposure of the different coated panels for samples + CS2, ○ CS2 + P25 (1 wbp%), □ CS2 + P25 (5 wbp%), ◊ CS2 + P25 (10 wbp%), Figure S2: SEM micrographs of the surface of the panels coated with formulated paints containing CS2 + P25 as binder before and after the weathering tests, Figure S3: SEM micrographs of the surface of the panels coated with non pigmented paints containing CS2 + JM as binder before and after the weathering tests. Figure S4: TEM micrographs of the cross-sections of the film obtained by casting the blend CS2+JM containing 10 wbp% TiO_2.

Acknowledgments: Financial support from the European Union (Limpid project FP7NMP-2012-2.2-6-310177), Ministerio de Economía y Competitividad (MEC, Ref. CTQ2014-59016-P), the Basque Government (GV IT-303-10)

and Gipuzkoako Foru Aldundia (EXP 55/14) is gratefully acknowledged. The SGIKER UPV/EHU for the electron microscopy facilities of the Gipuzkoa unit is also acknowledged. G. P. Leal is acknowledged for the SEM analysis. The Swiss National Science Foundation (SNF) Project No 200021-143283/1 is also gratefully aknowledged.

Author Contributions: Audrey Bonnefond, Edurne González, José M. Asua and Jose R. Leiza synthesized the latexes, prepared the blends, made the films and wrote the paper; Eliana Ieva, Giulio Brinati, Serena Carella, Alessio Marrani and Alessandro Veneroni synthesized the P(VDF-*co*-HFP) seed latex, formulated the paints and carried out the weathering tests ; John Kiwi, Cesar Pulgarin and Sami Rtimi carried out the photocatalytic activity tests.

References

1. Fujishima, A.; Zhang, X.T. Titanium dioxide photocatalysis: Present situation and future approaches. *C. R. Chimie* **2006**, *9*, 750–760. [CrossRef]
2. Allen, N.S.; Edge, M.; Verran, J.; Stratton, J.; Maltby, J.; Bygott, C. Photocatalytic titania based surfaces: Environmental benefits. *Pol. Degrad. Stab.* **2008**, *93*, 1632–1646. [CrossRef]
3. Cappelletti, G. TiO_2 nanoparticle: Traditional and novel synthetic methods for photocatalytic paint formulations. In *Nanoparticles: Properties, Classification, Characterization, and Fabrication*; Kestell, A.E., DeLorey, G.T., Eds.; Nova Science Publishers: New York, NY, USA, 2010; pp. 213–254.
4. Fujishima, A.; Rao, T.N.; Tryk, D. Titanium dioxide photocatalysis. *J. Photochem. Photobiol. C* **2000**, *1*, 1–21. [CrossRef]
5. Sunada, K.; Watanabe, T.; Hashimoto, K. Studies on photokilling of bacteria on TiO_2 thin film. *J. Photochem. Photobiol. A* **2003**, *156*, 227–233. [CrossRef]
6. Herrmann, J.M. Heterogeneous photocatalysis: State of the art and present applications in honor of Pr. R.L. Burwell Jr. (1912–2003), Former Head of Ipatieff Laboratories, Northwestern University, Evanston (Ill). *Top. CataL.* **2005**, *34*, 49–65. [CrossRef]
7. Linsebigler, A.L.; Lu, G.; Yates, J.T. Photocatalysis on TiO_2 Surfaces: Principles, Mechanisms, and Selected Results. *Chem. Rev.* **1995**, *95*, 735–758. [CrossRef]
8. Qu, X.; Alvarez, P.J.J.; Li, Q. Applications of nanotechnology in water and wastewater treatment. *Water Res.* **2013**, *47*, 3931–3946. [CrossRef] [PubMed]
9. Hochmannova, L.; Vytrasova, J. Photocatalytic and antimicrobial effects of interior paints. *Prog. Org. Coat.* **2010**, *67*, 1–5. [CrossRef]
10. Baudys, M.; Krýsa, J.; Zlámal, M.; Mills, A. Weathering tests of photocatalytic façade paints containing ZnO and TiO_2. *Chem. Eng. J.* **2015**, *261*, 83–87. [CrossRef]
11. Chen, J.; Poon, C.-S. Photocatalytic construction and building materials: From fundamentals to applications. *Build Environ.* **2009**, *44*, 1899–1906. [CrossRef]
12. Guarino, M.; Costa, A.; Porro, M. Photocatalytic TiO_2 coating to reduce ammonia and greenhouse gases concentration and emission from animal husbandries. *Bioresour. Technol.* **2008**, *99*, 2650. [CrossRef] [PubMed]
13. Maggos, T.; Bartzis, J.G.; Liakou, M.; Gobin, C. Photocatalytic degradation of NOx gases using TiO_2-containing paint: A real scale study. *J. Hazard Mater.* **2007**, *146*, 668–673. [CrossRef] [PubMed]
14. Tryba, B.; Homa, P.; Wróbel, R.J.; Morawski, A.W. Photocatalytic decomposition of benzo-[a]-pyrene on the surface of acrylic, latex and mineral paints. *Influence of paints composition. J. Photochem. Photobiol. A.* **2014**, *286*, 10–15. [CrossRef]
15. Tryba, B.; Homa, P.; Wróbel, R.J.; Morawski, A.W. Application of genetic algorithm for the simultaneous identification of atmospheric pollution sources. *Atmosph. Environ.* **2015**, *115*, 47–52. [CrossRef]
16. Gandolfo, A.; Bartolomei, V.; Gomez Alvarez, E.; Tilli, S.; Gligorovski, S.; Kleffmann, J.; Wortham, H. The effectiveness of indoor photocatalytic paints on NOx and HONO levels. *Appl. Catal. B.* **2015**, *166–167*, 84–90. [CrossRef]
17. Auvinen, J.; Wirtanen, L. The influence of photocatalytic interior paints on indoor air quality. *Atmosph. Environ.* **2008**, *42*, 4101–4112. [CrossRef]
18. Geiss, O.; Cacho, C.; Barrero-Moreno, J.; Kotzias, D. Photocatalytic degradation of organic paints constituents-formation of carbonyls. *Build Environ.* **2012**, *48*, 107–112. [CrossRef]
19. Al-Katan, A.; Wichser, A.; Vonbank, R.; Brunner, S.; Ulrich, A.; Zuind, S.; Novack, B. Release of TiO_2 from paints containing pigment-TiO_2 or nano-TiO_2 by weathering. *Environ. Sci. Processes Impacts.* **2013**, *15*, 2186–2193. [CrossRef] [PubMed]

20. Bonnefond, A.; González, E.; Asua, J.M.; Leiza, J.R.; Kiwi, J.; Pulgarin, C.; Rtimi, S. New evidence for hybrid acrylic/TiO_2 films inducing bacterial inactivation under low intensity simulated sunlight. *Coll. Surf. B* **2015**, *135*, 1–7. [CrossRef] [PubMed]
21. González, E.; Bonnefond, A.; Barrado, M.; Casado Barrasa, A.M.; Asua, J.M.; Leiza, J.R. Photoactive self-cleaning polymer coatings by TiO_2 nanoparticle Pickering miniemulsion polymerization. *Chem. Eng. J.* **2015**, *281*, 209–217. [CrossRef]
22. Lin, S.C.; Argasinski, K. Fluoropolymer Alloys. In *Fluoropolymers 2*; Hougham, G., Patrick, E.C., Johns, K., Davidson, T., Eds.; Kluwer Academic Publisher: New York, NY, USA, 1999; pp. 121–136.
23. Marolt, T.; Škapin, A.S.; Bernard, J.; Živec, P.; Gaberšček, M. Photocatalytic activity of anatase-containing facade coatings. *Surf. Coat. Technol.* **2011**, *206*, 1355–1361. [CrossRef]
24. Iezzi, R.A. Fluoropolymers Coatings for Architectural Application. In *Modern Fluoropolymers*; Scheirs, J., Ed.; John Wiley & Sons: Victoria, Australia, 1997; Chap.14; pp. 271–300.
25. Mc Keen, L.W. *Fluorinated Coatings and Finishes Handbook*; William Andrew: Norwich, NY, USA, 2006.
26. Koleske, J.V. *Paint and Coating Testing Manual 15th Edition of the Gardner-Sward Handbook*; ASTM International: West Conshohocken, PA, USA, 2012.